Tellus (2001), 53B, 306–321
Printed in UK. All rights reserved

TELLUS
ISSN 0280–6509

A climatological study of polar stratospheric clouds (1989–1997) from LIDAR measurements over Dumont d'Urville (Antarctica)

By VINCENZO SANTACESARIA[1]*, A. ROBERT MACKENZIE[2] and LEOPOLDO STEFANUTTI[1],
[1]*Istituto di Ricerca sulle Onde Elettromagnetiche, CNR, Via Panciatichi 64, 50127, Florence, Italy;*
[2]*Environmental Science Department, Lancaster University, Lancaster, LA1 4YQ, UK*

(Manuscript received 18 November 1999; in final form 8 December 2000)

ABSTRACT

Backscatter lidar data from the French Antarctic base in Dumont d'Urville (66.40°S, 140.01°E), including aerosol background and observations of polar stratospheric clouds (PSCs), have been collected since 1989. In the present work we present a climatological study of PSCs, using a data base consisting of almost 90 observations. The seasonal evolution of PSCs, their optical classification, and their relationship with the observation temperature were studied. The first PSC was observed on day number 175 (15 June) and the last on day number 260 (7 September). The characteristic mid-cloud altitude decreases through the season at a rate of 2.5 km/month. Type Ia, Ib, and II PSCs — identified by their optical properties — have been observed. External mixtures of these types have also been observed. These observations have been related to the local temperature measured by radiosondes. The relationship between PSC type and the period of the winter season was also investigated. Mixed (solid and liquid) type I clouds are mostly observed at the beginning of the winter. Type II clouds are observed only during the coldest period around midwinter, although temperatures below the frost point begin earlier and persist longer than this. Type Ia, solid-particle, clouds are observed mostly at the end of the winter.

1. Introduction

The discovery of the stratospheric ozone depletion over Antarctica was reported in the mid-1980s (Farman et al., 1985). Polar stratospheric clouds (PSCs) were quickly implicated in the ozone depletion (Crutzen and Arnold, 1986; Toon et al., 1986; Solomon et al., 1986). Heterogeneous chemical reactions on, or in, PSCs prepare the air for ozone destruction by converting chlorine reservoir species, which are relatively inert in the gas phase, into more reactive forms. PSCs are also responsible for denitrification, i.e., the removal of odd-nitrogen compounds from the lower stratosphere (Toon et al., 1986; Wofsy et al., 1990; Toon et al., 1990; Fahey et al., 1990).

PSC particles can be separated into two categories: those clouds formed above the frost point of the lower stratosphere (type I), and those formed at temperatures below the frost point (type II). Type I clouds can be further subdivided, according to their physical features (Toon et al., 1990). A type Ia cloud is composed of solid particles, while a type Ib cloud is composed of liquid particles (Fiocco et al., 1997).

The thermodynamic constraints on PSC formation are now reasonably well understood (Crutzen and Arnold, 1986; Toon et al., 1986; Worsnop et al., 1993; Carslaw et al., 1994). It is clear, however, that the kinetics of cloud formation can often be important, particularly for clouds com-

* Corresponding author.
e-mail: santac@iroe.fi.cnr.it

posed of solid particles (MacKenzie et al., 1995, 1997, 1998). This kinetic limitation may operate on the time-scale of hours-to-days, and so be observed in trajectory thermal histories (Tabazadeh et al., 1994; Larsen et al., 1996), or it may operate on time-scales well below those that can be resolved by operational meteorological analyses (Meilinger et al., 1995). Crutzen and Arnold (1986) proposed that type Ia PSCs are composed of nitric acid trihydrate (NAT), which is the most thermodynamically stable phase at stratospheric temperatures and vapour pressures. Tabazadeh et al. (1994), and Carslaw et al. (1994) proposed that type Ib PSCs are composed of supercooled ternary $HNO_3/H_2O/H_2SO_4$ solution droplets. In laboratory experiments, amorphous glassy solid particles have also been observed (Koehler et al., 1992). The formation mechanisms for type Ia and Ib is not clear, and different hypotheses on the formation of NAT and supercooled ternary solution (STS) have been suggested (Koop et al., 1997; Tabazadeh et al., 1994, 1995). Type II PSCs are observed for temperatures below the frost point and are composed principally of water ice crystals.

The first regular observations of PSCs were those performed by the Stratospheric Aerosol Measurements sensor (SAM) (McCormick et al., 1982; McCormick et al., 1989) installed on board the Nimbus 7, before the discovery of the ozone hole. Since 1988, ground-based LIDAR regular observations have been performed systematically by stations located on the Antarctic continent (Stefanutti et al., 1991; Adriani et al., 1992; Fiocco et al., 1992). PSC observations were performed also by airborne lidar (Browell et al., 1990; Poole et al., 1990). Also balloon-borne backscattersondes operating at different wavelengths were used in the analysis of PSC clouds (Rosen et al., 1989; Hofmann et al., 1991; Deshler et al., 1994). In situ measurements performed by means of the ER2 aircraft (Dye et al., 1992) contributed significantly to the evolution of PSC theory.

The first PSC climatology was made using SAM II data, using observations from 1978 to 1989 (Poole and Pitts, 1994). More recent satellite observations of PSCs have been made using the Polar Ozone and Aerosol Measurements (POAM II) sensors (Fromm et al., 1997). In this case, data from 1994 to 1996 are available. In this paper we present a PSC climatological study, using ground-based LIDAR measurements made from 1989 to 1997 at the Antarctic station Dumont d'Urville (66.40°S, 140.01°E). We focus on the seasonal variation during volcanically-quiescent periods — i.e., before the eruption of Mt. Pinatubo in June 1991 and after the decay of the volcanic aerosol. The effects of the volcanic aerosol have been studied by David et al. (1998), who performed a similar analysis to that below, but using a shorter data set from Dumont d'Urville. They have developed a method to identify the PSCs in the LIDAR signals in the presence of a strong volcanic aerosol load. The present paper complements the study of David et al. (1998) by focusing on volcanically unperturbed cases.

2. Experimental set-up and data management

The experimental site was at the French base of Dumont d'Urville (66.40°S, 140.01°E) on Antarctica. The LIDAR system used was developed jointly by IROE CNR and SA-CNRS (Stefanutti et al., 1992) as part of the POLE (Polar Ozone Lidar Experiment) project. The system measures several parameters involved in the ozone chemistry of the stratosphere: the ozone vertical distribution, the upper stratospheric temperature, aerosol scattering, PSC scattering and high altitude tropospheric clouds. The transmitter is based on a Nd:YAG laser and an XeCl excimer laser. A total of five different wavelengths are available (Stefanutti et al., 1992). Unfortunately, due to problems in the configuration of the system, we are able to use only the 532-nm channel in the present study. At 532 nm, the pulse energy is about 400 mJ with a pulse repetition rate of 10 Hz and a divergence of 0.5 mrad. The receiver is based on a 0.8-m diameter telescope with a 0.6 mrad field of view and equipped with two orthogonally polarised channels for the "s" and "p" direction.

The system is operated continuously by the staff of the base during the whole year. The LIDAR measurements are complemented by daily launch of meteorological radiosondes, which provide profiles of temperature, pressure, and wind vector. The average temperature uncertainty related to the radiosondes is estimated to be 1–1.5 K for altitudes between 16 and 20 km (David et al., 1998). Unfortunately, the sondes often do not reach far into the lower stratosphere, and so limit our analysis. However, there are enough LIDAR observations supported by radio-soundings to generate meaningful statistics. For this reason we prefer not to substitute the missing temperature data with satellite-derived data or meteorological analyses, which could include a significant bias (Pullen and Jones, 1997). Using the same source for all temperature profiles ensures data homogeneity.

From 1989 to 1997, 10 000 lidar profiles were collected. Each one was inverted using a simple inversion method developed at IROE (Morandi, 1992). This software is based on a modified backward Klett routine (Klett, 1981, 1985; Fernald, 1984). The output of the analysis is the aerosol backscatter coefficient profile for both p and s polarisation planes (B_p and B_s, respectively), and the scattering ratio (SR) calculated by using the following formula:

$$\mathrm{SR} = 1 + B_a/B_m, \tag{1}$$

where B_a is the total aerosol backscattering coefficient and B_m is the clear atmosphere backscatter coefficient. The errors in SR are strongly related to fluctuations in the signal detection, to arbitrary assumption of a SR equal to 1 to the base and top of the cloud layer which induce an error which can be estimated to be around 10% (Del Guasta et al., 1993; Chazette et al., 1995; David et al., 1998).

Important information about the classification of PSCs, and on their microphysical properties, can come from the depolarised signal, which is defined as (Stefanutti et al., 1991):

$$\Delta = \frac{B_s}{B_s + B_p}, \tag{2}$$

where B_s and B_p are the aerosol backscatter coefficients on the two polarisation planes, s and p, respectively. Other possible definitions for the depolarisation are used in the literature. The relationship among the various Lidar linear depolarisation definitions (including (2)) is reported in Cairo et al. (1999). As stated in Del Guasta et al. (1993), the error in the depolarisation profiles is around 20% when the effects of multiple scattering are neglected.

Each profile was checked for the presence of PSCs. The criteria used considered all clouds observed above the local tropopause to be PSCs. The tropopause level was determined by the temperature profiles obtained by the radiosondes, defined as the altitude at which the temperature lapse rate becomes less than 2 K km^{-1}.

To identify the clouds, we used the backscatter profiles; each increase in the signal over the aerosol background was assumed to correspond to a stratospheric cloud. This method is unreliable in the case of strong stratospheric volcanic aerosol loading, such as in the case of the Pinatubo aerosol in 1992, or, more generally, where large horizontal gradients in aerosol exist. The Pinatubo volcanic aerosol constituted a very high "aerosol background" against which it was not possible to detect PSCs on the basis of their backscattering alone. The background aerosol is assumed to be composed of spherical particles, an assumption that LIDAR measurements support (Stein et al., 1994; Chazette et al., 1995), and is assumed to have a mean radius of between 0.1–0.7 μm and they do not depolarise. This means that the formation of a liquid PSC, by the take-up of HNO_3, cannot be directly detected inside the eruption cloud. This is not the case for solid PSCs (at least those composed of aspherical particles), which are detectable by looking at the depolarisation.

The second step in the analysis procedure was to detect the presence of different layers or clouds in the same lidar profile. The cloud base and top were recorded for each of the layers identified. The mid-cloud altitude, M, was computed by means of the aerosol backscatter profile, using the following formula:

$$M = \frac{\int B_a(z) z \, dz}{\int B_a(z) \, dz}, \tag{3}$$

where $B_a(z)$ is the total aerosol backscatter coefficient, and z is the altitude. Hence, the data base for each cloud consists of: (i) the altitude and temperature of the mid-cloud, of the peak scattering ratio, and of the cloud base and top; (ii) the peak and mean depolarisation of the cloud; (iii) the cloud-integrated backscatter; and (iv) the peak and mean scattering ratios.

Each year contributes a different number, depending on the tropospheric conditions (thick, low, tropospheric clouds prevent transmission of the LIDAR beam into the lower stratosphere), on the member of staff operating the system, on the stratospheric temperature, and on the stratospheric aerosol loading.

Years 1991 and 1992 are almost totally missing,

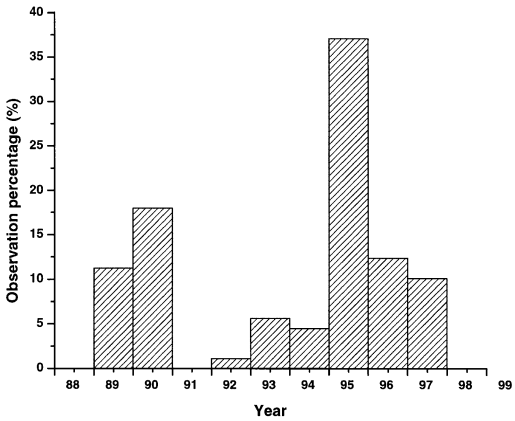

Fig. 1. Number of clouds observed for each year over Dumont d'Urville. During 1992, more clouds than those reported in the plots were observed (they were not considered in the analysis because of the strong background aerosol loading, which made the PSCs difficult to identify).

due to the unreliability of the data in these years. The problem of distinguishing PSCs from the Pinatubo eruption cloud in 1992 is discussed above. In 1991, the system was mis-aligned, producing only qualitative data. The year with the highest number of observations was 1995, which is the coldest year in our data set. The total count of PSC radiosonde-supported observations is 90 (Fig. 1).

3. Meteorological overview

The presence of a polar vortex is very important in the development of ozone depletion (Schoeberl and Hartmann, 1991). The vortex strongly decreases the poleward heat flux in the lower stratosphere, helping to maintain low temperatures and high probabilities of PSC formation. The vortex, therefore, can contain air parcels that have been activated for ozone destruction. A strong gradient of potential vorticity characterises the polar vortex edge.

The French base Dumont d'Urville (DDU) is located on the shore of the bay of the Ross Sea. During the winter season, its position is underneath the edge of the polar vortex (Santacesaria et al., 1999). Stratospheric temperatures at DDU are, therefore, not as low as at stations underneath the centre of the vortex. Generally, the station can be considered inside the vortex from June to October of each year. Due to its position with respect to the vortex, the PSC season is not uniform, but is perturbed by minor warming phenomena associated with vortex deformations.

Stratospheric temperatures above DDU from June to October can reach values which are well below the nominal NAT existence temperature, T_{nat} and the nominal ice frost point, T_{i}, where both are calculated assuming constant vapour mixing ratios of 10 ppbv for nitric acid and 5 ppmv for water. Fig. 2a shows the distribution of radiosondes that experienced temperatures below the NAT existence temperature during the whole winter season, indicating that they are present from the end of June (day 180) to the end of September (day 270). The coldest period, with the temperature 6°C or more below T_{i}, is observed, in our data set, in a period ranging from the 20 July (day 200) to the end of August (day 240) (Fig. 2b).

Fig. 3 shows the mean temperature vertical distribution during the vortex season. This plot has been obtained by using all the radiosondes available for the period of our study. It can be observed that when the polar vortex starts, the colder temperatures are observed at high altitudes around 25 km. As the season develops, the entire lower stratosphere becomes very cold and the minimum temperatures are observed at lower altitudes. This condition is interrupted abruptly when the polar vortex no longer covers the station, around the end of September and the beginning of October (day 270). As one would expect from the wintertime zonal circulation, the winds over DDU are westerly in the lower stratosphere, and can be very intense, reaching speeds of up to $100\ \mathrm{m\ s^{-1}}$.

4. Results and discussion

We have divided this section into 3 different parts. The first part deals with general aspects of the seasonal evolution of PSCs, showing the observations as a function of altitude, and the seasonal march of the cloud frequency distribution. In the second part we present the classification of the clouds according to their optical characteristics. In the third part we discuss the relationship

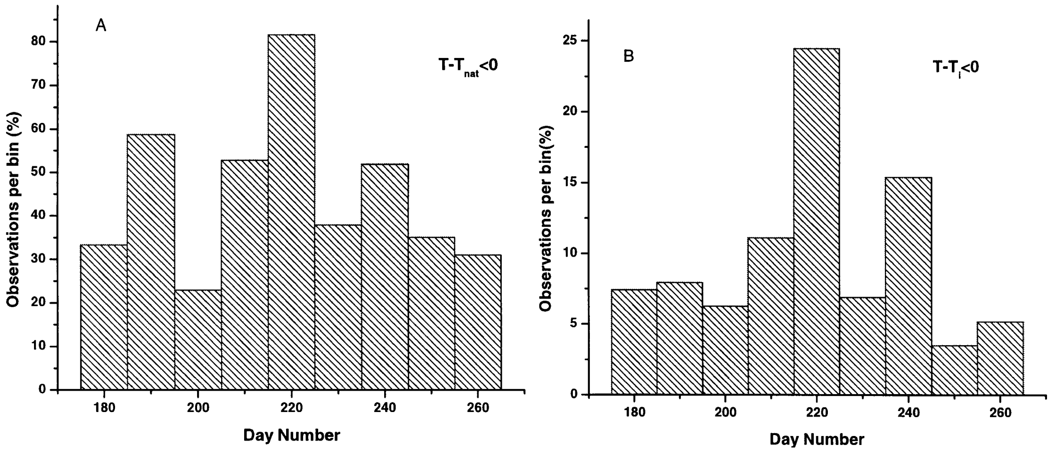

Fig. 2. Percentage of temperature observations below PSC temperature thresholds, as a function of day number, retrieved from all the radiosondes available over Dumont d'Urville In panel A, the threshold temperature is the NAT-point, T_{nat}, calculated assuming 10 ppbv nitric acid and 5 ppmv total water. In panel B, the threshold temperature is the frost point, T_i, calculated assuming 5 ppmv of total water.

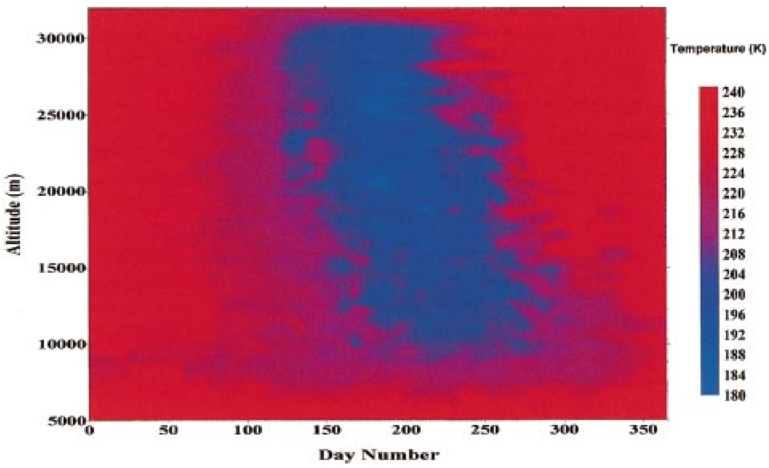

Fig. 3. Temperature, as a function of altitude and of day number, obtained using all the radiosondes available in the period 1989–1997. The altitude of the minimum temperature decreases with time.

between the cloud observations and the existence temperatures for NAT and ice.

4.1. *Seasonal variations in cloud frequencies height*

Fig. 4 shows the distribution of PSC observations as a function of day of the year. In our data set, the earliest observation corresponds to 25 June (day number 175) and the latest one corresponds to 20 September (day number 260). Most of the observations occur over a period ranging between the end of June (day 180) and the end of August (day 240). Towards the end of the season, after day 230, the frequency of observation is lower, even though temperatures remain at or near the nominal frost point well beyond this date. This is probably due to the fact that, as is discussed below, dehydration and denitrification of the polar stratosphere has taken place (Rosen et al., 1991), lowering the actual frost point and NAT point.

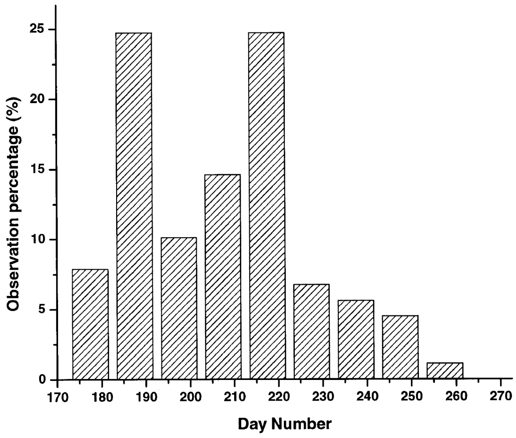

Fig. 4. Percentage of all lidar observations that show PSCs, as a function of day number. The percentage of PSCs in the observations decreases after the end of August (day number 243).

LIDAR observations at other sites in Antarctica (Adriani et al., 1992) did not observe PSCs after August.

The long-term PSC observations reported by McCormick et al. (1989) were made using the SAM II single channel sun photometer (measuring at a wavelength of 1 μm).The SAM II PSC climatology is based on the analysis of the aerosol extinction ratio together with ancillary measurements of Geopotential height and temperature profiles. Measurements are possible only in daylight, and so are not necessarily representative of the regions in polar night. However, for the latitude of DDU, the SAM II data has sufficient coverage to make a useful a comparison with the present study. McCormick et al. (1989) report the earliest PSC observations in late May and the latest observations in late September or early October.

Poole et al. (1994) developed a longer climatology based on SAM II observations from 1978 to 1989. According to this climatology, Antarctic PSCs are typically observed from mid-May to early November. They also showed how, for the longitude of DDU (140°E), the probability of sighting a PSC is lower compared to longitudes closer to the Greenwich Meridian where the maximum probability and the coldest temperatures are located. Moreover, as discussed above, DDU is located under the edge of the polar vortex (Santacesaria et al., 1999), where the fluctuations of the vortex itself could produce a warming of the local stratosphere, hence decreasing the probability of observing PSCs. This might explain why we observe a shorter PSC season over Dumount d'Urville compared to the zonal satellite climatology. Like Poole et al. (1994), we find a maximum probability in sighting PSCs in August.

Fromm et al. (1997) provided another climatology for the years 1994 to 1996. They used POAM II solar occultation measurements. POAM II has the same polar orbit as SAM II, but measures to within 2° latitude of the south pole. The results of Fromm et al. (1997) generally agree with those of Poole et al. (1994) and this study, with the maximum in the frequency of observation occurring in August.

Fig. 5 shows the mid-cloud altitude, calculated using (3), as a function of day number. The variation bars indicate the base and the top of the cloud. A general trend in the lowering of the cloud altitude — measured as mid-cloud, cloud-top, or cloud-bottom altitude — is clearly visible. We observe the first PSC clouds at a mid-cloud altitude around 22 km (Fig. 5). Later PSCs are observed below 15 km and, in some cases, are located just above the tropopause. The apparent rate of descent is approximately 2.5 km per month. A similar trend is calculated using the altitude of the base or the altitude of the top of the PSC cloud. This descent could be explained by a combination of three effects: diabatic descent of air within the polar vortex, which moves the maxima in the HNO_3 and H_2O distributions to lower altitude (Rosen et al., 1993); sedimentation of particles from the early, high-altitude, PSCs, which redistributes HNO_3 and H_2O from higher to lower altitudes; and a decrease in the altitude at which the minimum stratospheric temperature occurs. In a previous study of ozone data from the DDU lidar (Santacesaria et al., 1999), we found diabatic descent rates of about 0.25 km per month, in good agreement with the calculated diabatic descent rates of Rosenfield et al. (1994). Fig. 3, which shows a linear descent rate of about 5 km per month, suggests that the descent of the temperature minimum occurs relatively quickly. Vertical redistribution of HNO_3 and H_2O through particle sedimentation will be a sporadic process, with rates varying greatly with particle size. Type II particles can have fall speeds approaching

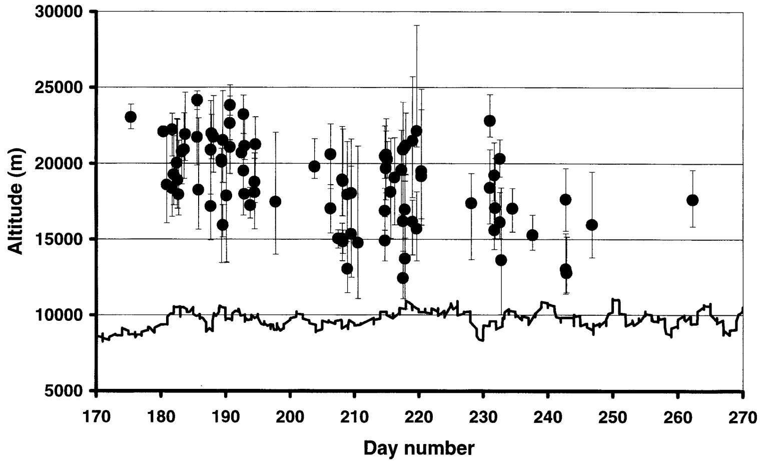

Fig. 5. Mid-cloud altitude (see eq. (3)) of each PSCs observed, as a function of day number. For each point a variability bar indicates the base and the top of each cloud. The altitude of the tropopause is also reported in the plot (thin line).

1 km h^{-1} (Turco et al., 1989). Our apparent rate of descent of the altitude of cloud observation is probably due, therefore, to the action of the three processes above, all acting on different timescales.

McCormick et al. (1989), David et al. (1998), and Fua et al. (1992) also observed a lowering in the altitude of PSCs as winter progresses. Poole et al. (1994) observed PSCs from SAM II in the altitude range 15–22 km, with a lowering towards the end of the season. Fromm et al. (1997) also measured a range of 17.4–23.5 km, with a lowering of approximately 2 km per month, somewhat slower than that deduced from our measurements.

Fig. 5 also shows the mean tropopause altitude. After day 210 (end of July), the PSC clouds are often within 1 km of the tropopause. This may be significant in the context of dehydration and denitrification (Wofsy et al., 1990; Toon et al., 1990; Gobbi et al., 1993). This process is not well understood, but it is assumed that the water and the nitric acid condensed in the larger particles are removed by gravitational settling. When these larger particles are formed at a high altitude they can evaporate before leaving the stratosphere, releasing the condensed vapours. This can increase the threshold temperature for PSC formation in the lower layers. Also, because mixing of polar air with that of the middle latitudes is more likely at potential temperatures below about 400 K, the water vapour and nitric acid sedimented from above is available to be mixed out to lower latitudes (Tuck et al., 1996). When the PSCs form at lower altitudes (i.e., close to the tropopause), the condensed matter is removed completely from the stratosphere. In some cases we have observed cirrus directly connected to overlying PSCs.

Fig. 6 shows the frequency of the observation as a function of temperature. The highest frequency occurs around 189 K, but high values are present also for temperatures around 196 K. Poole et al. (1994) observed the highest sighting

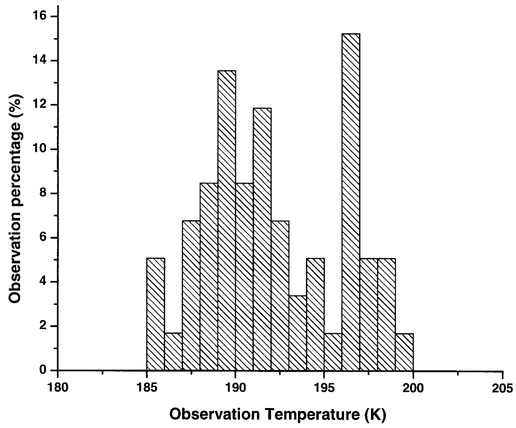

Fig. 6. Percentage of PSC observations as a function of mid-cloud temperature.

probability around 190 K, again demonstrating agreement between the climatologies. No PSCs were observed for temperatures above 200 K in our dataset. There may be a bias at the lower end of our temperature range, caused by radiosonde balloons bursting, limiting the number of observations at high altitudes.

In all our seasonal analysis, and at the level of our comparison, no trend is discernible in the several PSC climatologies that we have compared, covering the years 1978–1997.

4.2. PSC classification

A general classification of the clouds can be made using the observed scattering ratios and depolarisations. PSCs are currently divided into three categories: types Ia, Ib and II (Browell et al., 1990; Toon et al., 1990; Stefanutti et al., 1991). To summarize, type Ia PSCs are characterized by a low scattering ratio and high depolarisation. They are assumed to be formed by non-spherical particles, of 1–2 μm radius (Toon et al., 1990b). Clouds of type Ib have a moderate backscatter ratio and low depolarisation. Toon et al. (1990b), suggested that type Ib clouds comprise spherical particles with a radius of around 0.5 μm. Type II clouds are characterised by a high backscattering ratio and moderate depolarisation (Table 1). Evidence that indicates the presence of other PSC categories not included in the original Browell classification, has been found recently (Tsias et al., 1999; Stein et al., 1999).

In Fig. 7, we have plotted, for each cloud system observed, the mean value of the aerosol depolarisation against the peak scattering ratio. In the same plot, standard deviations for the two variables are also reported. Points without bars are related to a single observation. Finally each point is colour-coded by the day number during which it has been observed.

Table 1. *Classification of PSC based on their scattering ratio and depolarisation (after Browell et al. (1990))*

PSC type	Scattering ratio	Aerosol depolarisation (%)
Ia	1.5	25–50
Ib	3–6	<2.5
II	>10	>9

Different types of PSC are prominent in Fig. 7. Type Ib clouds are represented by those points with a very low depolarisation and a scattering ratio of up to 5. The points with a very high scattering ratio (up to 30) and a depolarisation around 10% can be classified as type II PSCs. The highly variable scattering ratios but relatively low variability of depolarisation for type II PSCs suggests that the phase and shape of type II particles is relatively constant. The variation in the scattering ratio in our data is then primarily due to changes in the number or the size of scattering particles. Clouds with a very low scattering ratio (less than 2) but a high depolarisation (up to 50%) are also present (i.e., type Ia).

Along with the various PSC types, Fig. 7 shows other data that do not obviously belong to any of the three types. Rosen et al. (1993) suggested that the three-type classification is a generalisation, and that types Ia and Ib are only two easily identifiable extremes of what is, in reality, a continuum or combination of the two. Our results show that, whilst not all of the backscatter-depolarisation space is occupied by the observations, there is a substantial range of the optical properties of PSCs. This range may be due to mixing of particles belonging to the canonical types, or due to particles which have physical properties not considered in the canonical types.

Assuming for the moment that the first of these hypotheses is correct, we use the multi-component optical model developed by Kent et al. (1990). Subtracting from the signal the molecular contribution by using Stefanutti et al. (1991), we get, for the case of highly depolarising and relatively low depolarising particles present in the same probed volume, the following expression for the aerosol depolarisation:

$$\Delta = \frac{R_y}{R_x + R_y}\Delta_y + \frac{R_x}{R_x + R_y}\Delta_x, \tag{4}$$

with

$$R_x = \frac{\beta_{\text{low}}}{\beta_{\text{m}}}, \qquad R_y = \frac{\beta_{\text{high}}}{\beta_{\text{m}}},$$

where Δ_y and β_{high} are the depolarisation and the backscattering coefficient due to high depolarising particles, Δ_x and β_{low} are related to low depolaris-

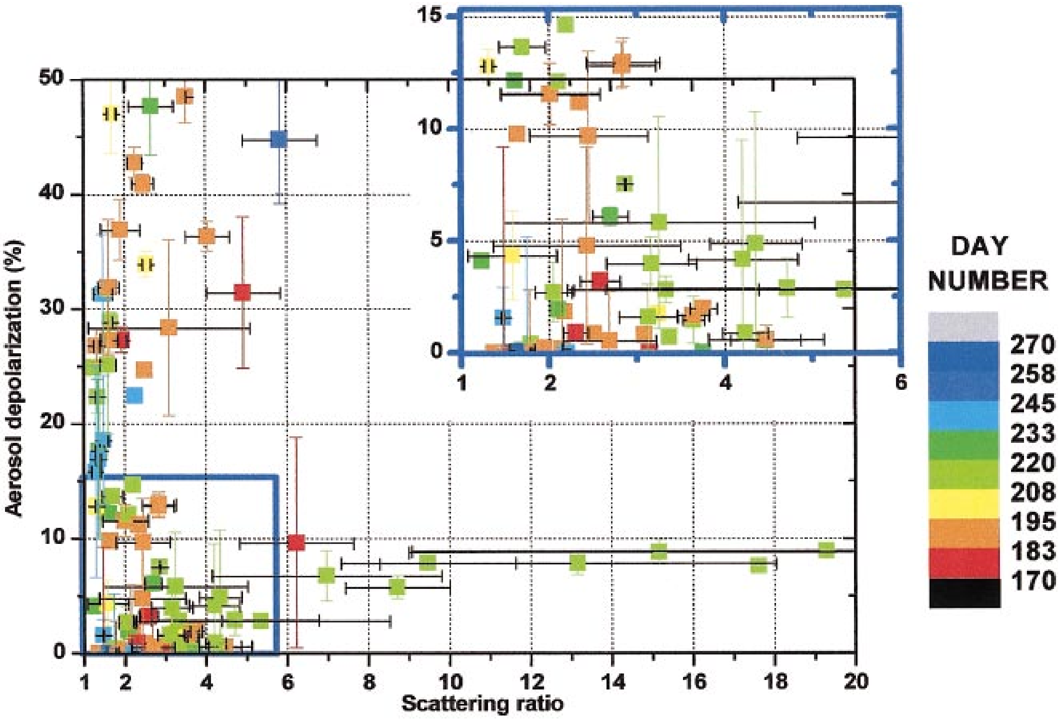

Fig. 7. Aerosol depolarisation (see eq. (2)) versus scattering ratio peak value, for each cloud system observed during the 8 years. The bars represent the variability of the two parameters within each cloud system. The points are segregated into different periods of the PSC season from day 175 to day 265, with a step of 12 days. The segregation is represented by the colour code; red colours indicate observations performed at the beginning of the PSC season, and blue colours those at the end. The inset shows an expanded plot of the region near the origin.

ing particles, and β_m is the backscatter coefficient of the molecular atmosphere.

Total depolarisation ranges between two extremes. One with $R_y \gg R_x$, where depolarisation is equal to Δ_y (i.e., high depolarising particles). The other with $R_x \gg R_y$, which produces a depolarisation exactly equal to Δ_x (i.e., zero in the liquid case). The other cases produce depolarisation ranging between Δ_x (i.e., zero) and Δ_y, with scattering ratio equal to $1 + R_x + R_y$. We can identify such mixed-cloud cases as those points in Fig. 7 with scattering ratio less than 10 and with depolarisation between 2.5% and 10%, as being a mixture of type Ib liquid particles and type II water ice particles.

Yet other points in Fig. 7 have a high value of the depolarisation (greater than 20%), typical of type Ia, and moderate scattering ratio (from 3 to 6), typical of type Ib. These points cannot be explained as a mixture of different types. One possibility is to assume a type of PSC not included in the canonical classification. This new type would be characterised by high depolarisation and moderate scattering ratios. Another possibility is to extend the Ia class to include moderate scattering ratios. Similar observations have been made also during the APE-POLECAT campaign (Stefanutti et al., 1999) by the airborne lidar OLEX which was installed on board of the DLR Falcon. By using a microphysical and optical model Tsias et al. (1999) suggest that such clouds comprise NAT particles rather closer to thermodynamic equilibrium than the particles that usually form type Ia clouds.

The seasonal variation in observations of the various cloud types is also reported in Fig. 7. Each value is colour-coded according to day number, from day 175 to day 265, in 12-day intervals. Before day number 205 (reddish points), the temperatures over the Antarctic region are below T_i, but in this period most of the clouds are either of type I (both a and b), or clouds that can be ascribed to the mixing of types Ia and Ib. When the temperatures are colder in the middle of the winter, from day numbers 205–225 (the first half of August) (greenish points), PSCs of type II are observed. Temperatures during that period are expected to be up to 6° below T_i. In the second part of the winter season, this type of PSC is no longer observed, probably because of a drier atmosphere. Type II PSCs are formed very close to the tropopause (Fig. 5). This low altitude, together with the occurrence of large ice crystals in type II clouds (Goodman et al., 1989), is expected to produce a strong dehydration and denitrification of the lower stratosphere (Wofsy et al., 1990; Toon et al., 1990). For the other part of the season (blueish points), type I clouds are again the predominant cloud system, including the new class of cloud with moderate scattering ratio. It is worth noting that mixed phase clouds are not observed in this period.

One possible explanation of the seasonal variation of type II PSC occurrences is that, even though T_i is well below the average temperature over the Antarctic region, temperature waves may regulate the creation of the PSCs over this region (De Rudder et al., 1996). According to the simulation of De Rudder et al. (1996), type II PSCs exist only for very short periods with a distribution that is quite complex compared to the type I PSCs. Their simulation produced type II PSCs from July until September, at a latitude of 75°.

Our observation that the first PSCs present are of type Ia or Ib, even though the temperature could allow the presence of type II, compares well with the analysis of De Rudder et al. (1996). It does not support the hypothesis of NAT nucleation via ice (Koop et al., 1995), at least in the Antarctic region. It appears from the DDU data that type Ia clouds, usually assumed to be composed of NAT, are formed before type II clouds, usually assumed to be composed of water ice, over the Antarctic region. This supports the hypothesis that solid PSC formation is due to the freezing of ternary solution droplets (Molina et al., 1993; Iraci et al., 1994). It is possible, of course, that ice clouds have been formed upwind of DDU, nucleating the NAT particles that are observed early in the season. Such a hypothesis could be studied using backward trajectories, but would be limited by the quality of the meteorological analysis in the Antarctic region.

4.3. *Temperature-resolved analysis*

In this section, we discuss the relationship between the physical characteristics of the clouds and the temperature at which they are observed. The static position of a ground-based instrument means that no information on air parcel thermal histories is directly observable. The threshold temperature for PSC existence depends on the atmospheric pressure at which the particle is located, so, in order to place all the data relative to a single origin, we refer all data to the local ice and NAT existence temperatures (T_{nat} or T_i). $T - T_{nat}$ is therefore the difference between the ambient temperature and the temperature of NAT crystallisation (Hanson et al., 1988), and $T - T_i$ is the difference between the ambient temperature and the ice frost point (Pruppacher and Klett, 1985), at the level at which the PSC is detected. T_{nat} is calculated using an assumed profile of HNO_3 (Gille et al., 1984) and T_i by assuming a value of water vapour in stratosphere equal to 5 ppm.

Due to bursting of the radiosonde balloons, not all sondes reached mid-cloud altitudes. As a consequence of this, the number of points showed in the following plot is roughly 30% less than in previous sections. In Figs. 8a, b, we report the histogram of cloud frequency observation versus $(T - T_{nat})$ and $(T - T_i)$ for the mid-cloud level. Most of the observations show a mid-cloud temperature below T_{nat}. Only 4% of the observations have a mid-cloud temperatures above T_{nat}. These few cases can be explained if the real HNO_3 or H_2O concentrations were different from those assumed in the computation of T_{nat}. A decrease in the observation frequency with temperature is observed.

In Figs. 9a, b, the variation of the mean peak scattering ratio for each cloud is shown, versus $(T - T_{nat})$ and $(T - T_i)$ respectively. In Fig. 9a, two lines indicate the error in the location of the zero point in $(T - T_{nat})$, assuming an error of $\pm 50\%$ in the HNO_3 and H_2O profiles. At high temperature we observe low values of the scattering ratio around 2. Those values are almost constant as the temperature decreases. Around 5–7 K below T_{nat}, higher values of the scattering ratio are obtained.

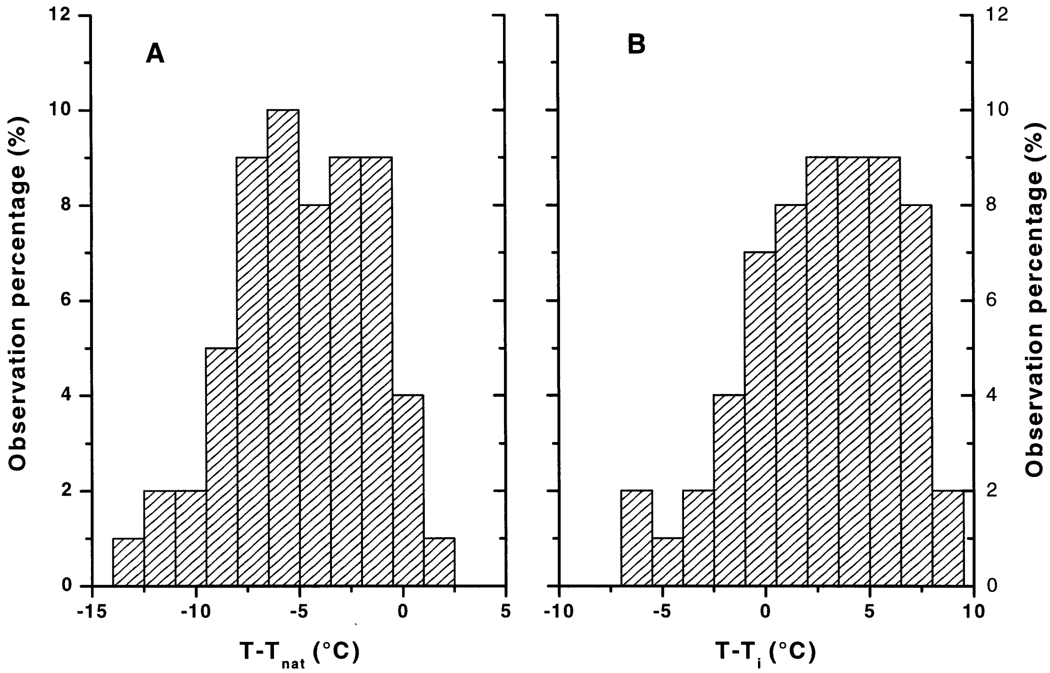

Fig. 8. Percentage of PSC observations as a function of the $T-T_{nat}$ (panel a) and $T-T_i$ (panel b).

Looking at the same plot, but relative to $(T-T_i)$, a strong increase in the scattering ratio is observed for temperatures below T_i, suggesting the creation of large ice crystals.

In Figs. 10a, b, the depolarisation data are plotted against $(T-T_{nat})$ and $(T-T_i)$. For temperatures close to T_{nat}, we observe high depolarisation (higher than 10%), furthermore non-depolarising clouds are also present. The two families of observations are distinct, and mixtures are not apparent. For temperatures between T_{nat} and $(T_{nat}-5)$, highly depolarising particles still exist, but with lower values. Non-depolarising particles are also present in this temperature range, but in this case the two groups cannot be well distinguished. Mixed clouds may therefore exist in this temperature range. Only at temperatures below T_i is the depolarisation expected for type II clouds observed. Liquid particles are also observed below T_i. Only at temperatures 2° below T_i do they disappear. The presence of solid particles above the nominal NAT existence point has been also observed by Adriani et al. (1995) and Gobbi et al. (1993), who found depolarisation enhancement well above the temperature of NAT over McMurdo station in Antarctica. One explanation is that large NAT particles, with radii of a few μm, although evaporating, could survive for days in unsaturated air (Turco et al., 1989; Peter et al., 1994).

In Fig 11, we present the mean backscattering coefficient (proportional to the total aerosol volume) versus $(T-T_i)$ for non-depolarising particles (i.e., depolarisation $<1\%$). An increased backscatter coefficient is observed with decreasing temperature from about 5 K below the NAT point, i.e., about 2 K above the ice frost point. These observations agree with Dye et al. (1992, 1997) who also observed an increase in the total particle volume for temperature approximately 5 K below T_{nat}. Their observations were based on in situ measurements over the Arctic (during the AASE I mission) and over the Antarctic (during the ASHOE/MAESA mission). The increase in total particle volume is explained (Tabazadeh et al., 1994; Carslaw et al., 1994) by uptake of HNO_3 and H_2O as temperatures drop.

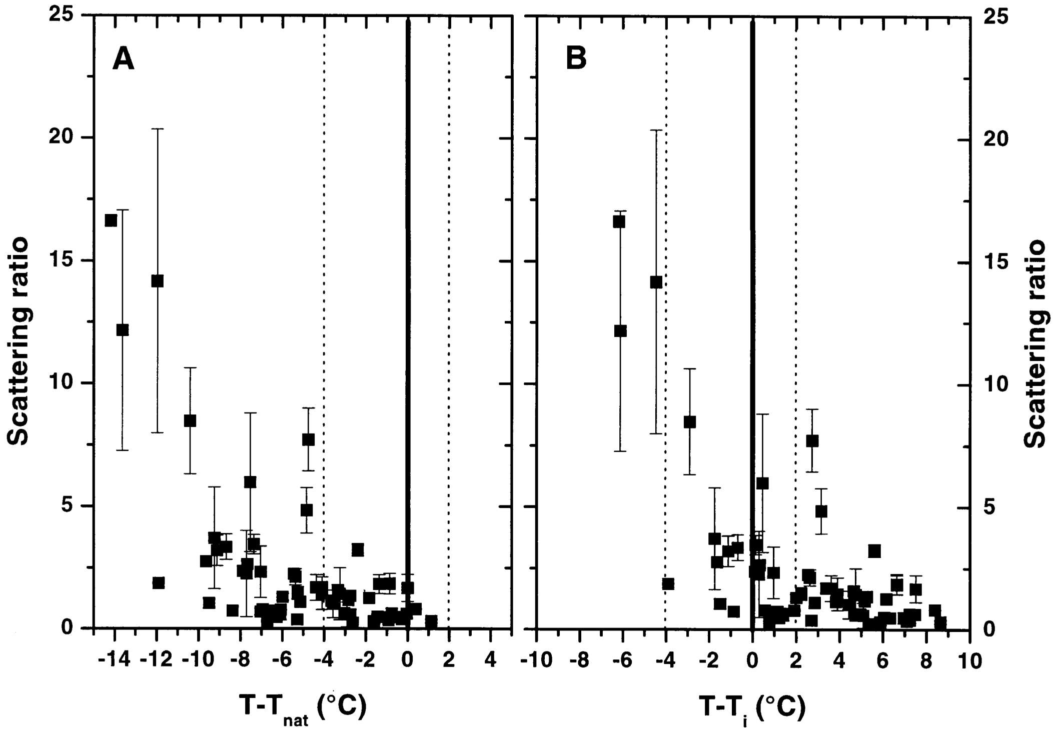

Fig. 9. Scattering ratio versus $T - T_{nat}$ (panel a) and $T - T_i$ (panel b), for each cloud system observed. The dotted lines above and below the zero represent the variation of the zero position for 50% errors in the H_2O and HNO_3 profiles used for the T_i and T_{nat} computations.

5. Conclusions

A PSC data set collected from 1989 to 1997, at the Antarctic station of Dumont d'Urville, has been presented in this paper. This data set shows that the probability of observing PSCs is fairly uniform during the first part of the winter season (up to the end of August) but during September there are few PSCs over our experimental site. We expect that PSC-induced dehydration and denitrification of the atmosphere account for this feature. Statistics on the altitude of the top, the base, and the middle of the clouds show a lowering of PSCs during the winter season. This confirms other long-term analyses for the Antarctic region. We observe an apparent rate of descent of around 2.5 km/month. The reason of this lowering could be ascribed either to a continuous redistribution of nitric acid from higher to lower altitudes, or due to the increase of the temperature at higher altitudes as observed by the radiosondes profiles (Fig. 3). These mechanisms are not, of course, mutually exclusive. The apparent decent rate seems to be a compromise between the descent rate of the temperatures, which from Fig. 3 can be estimated around 5 km/month, and the diabatic descent rate which, in the lower stratosphere, is around 0.5 km/month (Rosenfield et al., 1994).

This lowering of the PSC altitude during the winter also seems to affect the altitude where the ozone depletion starts over DDU. Ozone depletion is observed to start at high altitudes during midwinter and only later at lower altitudes (Santacesaria et al., 1999).

The different types of PSC reported in the literature have also been observed in our study, each identified by their optical properties. Cases that are best explained as a mixture of the classical PSC types have been observed. Mixtures of PSC types have been also observed by a lidar system

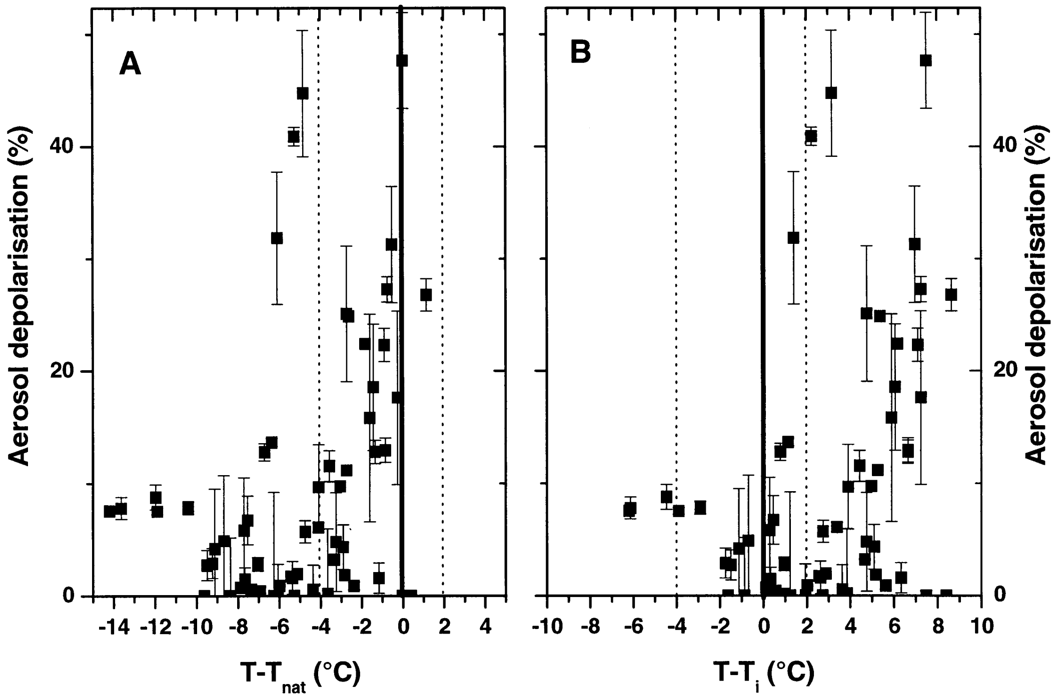

Fig. 10. Aerosol depolarisation versus $T - T_{nat}$ (panel a) and $T - T_i$ (panel b) for each cloud system observed. The dotted lines above a below the zero represent the variation of the zero position for 50% errors in the H_2O and HNO_3 profiles used for the T_i and T_{nat} computations.

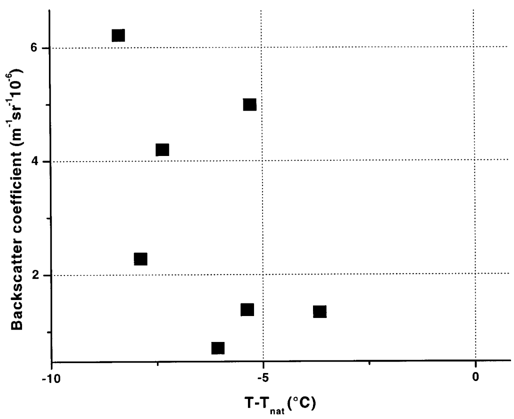

Fig. 11. Average backscattering coefficient versus $T - T_{nat}$ for the cloud systems with aerosol depolarisation below 1%.

installed in McMurdo during the winter of 1995 (Gobbi et al., 1998).

At the beginning of the winter season only type Ia or b are observed. Type II is observed only during the first part of August when the temperature observed by the radiosondes are colder. Later only type I is observed. Type Ia is present only for temperatures very close to T_{nat}. A strong increase of the scattering ratio is observed for temperatures 2 K above the ice frost point, and below, indicating a rapid increase in particle volume. Liquid particles are observed at temperatures below T_{nat}, and in some cases liquid particles are present at temperatures 2 K below T_i.

6. Acknowledgements

This study has been developed in the frame of an Italian-French POLE co-operative project between PNRA (National Program for Antarctic Research, Italy) and Institute Polaire Francaise. We wish to thank the Service d'Aeronomie du CNRS for their collaboration in the joint POLE programme management. We also wish to thank Donatella Guzzi, Marco Morandi and Massimo del Guasta, for their assistance, and all the teams who operated in the station for all these years. Support has been received by the EC Environment and Climate Programmes in the frame of the SAONAS project (Contract ENV4-CT95-0090).

REFERENCES

Adriani, A., Deshler, T., Gobbi, G. P., Johnson, B. J. and Didonfrancesco, G. 1992. Polar stratospheric clouds over McMurdo, Antartica during the 1991 spring: lidar and particle counter measurements. *Geophys. Res. Lett.* **19**, 1755–1758.

Adriani, A. Deshler, T., Didonfrancesco, G. and Gobbi, G. P. 1995. Polar stratospheric clouds and volcanic aerosol during spring 1992 over McMurdo Station, Antarctica: lidar and particle counter comparison. *J. Geophys. Res.* **100**, 25,877–25,897.

Browell, E. V., Butler, C. F., Ismail, S. Robinette, P. A., Carter, A. F., Hidgon, N. S., Toon, O. B., Schoeberl, M. R. and Tuck, A. F. 1990. Airborne LIDAR observation in the wintertime Arctic stratosphere: polar stratospheric clouds. *Geophys. Res. Lett.* **17**, 385–388.

Cairo, F., Di Donfrancesco, G., Adriani, A., Pulvirenti, L. and Fierli, F. 1999. A comparison of various linear depolarization parameters measured by lidar. *App. Optics* **38**, 4425–4432.

Carslaw, K. S., Luo, B. P., Clegg, S. L., Peter, T., Brimblecombe, P. and Crutzen, P. 1994. Stratospheric aerosol growth and HNO_3 gas phase depletion from coupled HNO_3 and water uptake by liquid particles. *Geophys. Res. Lett.* **21**, 2479–2482.

Chazette, P., David, C., Lefrere, J., Godin, S. and Megie, G. 1995. Comparative lidar study of the optical, geometrical, and dynamical properties of stratospheric post-volcanic aerosols, following the eruption of El Chichon and Mount Pinatubo. *J. Geophys. Res.* **100**, 23,195–23,207.

Crutzen, P. J. and Arnold, F. 1986. Nitric acid cloud formation in the cold Antarctic stratosphere: a major cause for spring time ozone hole. *Nature* **324**, 651–655.

David, C., Bekki, S., Godin, S., Megie, G. and Chipperfield, M. P. 1998. Polar stratospheric clouds climatology over Dumont d'Urville between 1989 and 1993 and the influence of volcanic aerosols on their formation. *J. Geophys. Res.* **103**, 22,163–22,180.

Del Guasta, M., Morandi, M., Stefanutti, L., Brechet, J. and Piquard, J. 1993. One year of cloud lidar data from Dumont d'Urville (Antarctica). 1. General overview of geometrical and optical properties. *J. Geophys. Res.* **98**, 18,575–18,587.

De Rudder, A., Larsen, N., Tie, X., Brassuer, G. P. and Granier, C. 1996. Model study of polar stratospheric clouds and their effect on stratospheric ozone. 1. Model description. *J. Geophys. Res.* **101**, 12,567–12,574.

Dye, J. E., Baumgardener, D., Gandrud, B. W., Kawa, S. A., Kelly, K. K., Lowenstein, M., Ferry, G. V., Chan, K. R. and Gary, B. L. 1992. Particle size distributions in Arctic polar stratospheric clouds, growth and freezing of sulphuric acid droplets, and implications for cloud formation. *J. Geophys. Res.* **97**, 8015–8034.

Dye, J. E., Baumgardener, D., Gandrud, B. W., Drdla, K., Barr, K., Fahey, D. W., Delnegro, L. A., Tabazadeh, A., Johnson, H. H., Wilson, J. C., Loewenstein, M., Podolske, J. R. and Chan, K. R. 1996. In situ observation of an Antarctic polar stratospheric cloud: similarities with Arctic observations. *Geophys. Res. Lett.* **23**, 1913–1916.

Fahey, D. W., Kelly, K. K., Ferry, G. V., Poole, L. R., Wilson, J. C., Murphy, D. M., Loewenstein, M. and Chan, K. R. 1989. In situ measurements of total reactive nitrogen, total water, and aerosol in a polar stratospheric cloud in the Antarctic. *J. Geophys. Res.* **94**, 11,299–11,315.

Fahey, D. W., Solomon, S., Kawa, S. R., Loewenstein, M., Podolske, J. R, Strahan, S. E. and Chan, K. R. 1990. A diagnostic for denitrification in the winter polar stratosphere. *Nature* **345**, 698–702.

Farman, J. C., Gardiner, B. G. and Shanklin, J. D. 1985. Large losses of total ozone in Antarctic reveal seasonal ClO_x/NO_x interaction. *Nature* **315**, 207–210.

Fernald, F. G. 1984. Analysis of atmospheric lidar observations: some comments. *Appl. Optics* **23**, 652–653.

Fiocco, G., Cacciani, M., Digirolamo, P., Fua, D. and De Luisi, J. 1992. Stratospheric clouds at south pole during 1988. 1. Results of lidar observations and their relationship to temperature. *J. Geophys. Res.* **97**, 5939–5946.

Fiocco, G., Larsen, N., Bekki, S., Di Sarra, A., David, C., Peter, T., Spreng, S. and MacKenzie, A. R. 1997. Particles in the stratosphere. In: *European Research on the Stratosphere: the contribution of EASOE and SESAME to our current understanding of the ozone layer*. EUR 16986, Office for Official Publications of the European Communities, Luxembourg, 61–91.

Fromm, M. D., Lumpe, J. D., Bevilacqua, R., Shettle, E., Hornstein, J., Massie, S. and Fricke, K. 1997. Observation of Antarctic polar stratospheric clouds by POAM II: 1994–1996. *J. Geophys. Res.* **102**, 23,659–23,672.

Fua, D., Cacciani, M., Di Girolamo, P., Fiocco, G. and Di Sarra, A. 1992. Stratospheric clouds at South Pole during 1988: 2. Their evolution in relation to atmospheric structure and composition. *J. Geophys. Res.* **97**, 5947–5952.

Gille, J. C. and Russel, J. M. 1984. The limb infrared monitor of the stratosphere: experiment description, performance and results. *J. Geophys. Res.* **89**, 5125–5140.

Gobbi, G. P. and Adriani, A. 1993. Mechanism of formation of stratospheric clouds observed during the Antarctic late winter of 1992. *Geophys. Res. Lett.* **20**, 1427–1430.

Gobbi, G. P., Di Donfrancesco, G. and Adriani, A. 1998. Phyisical properties of stratospheric clouds during the Antarctic winter of 1995. *J. Geophys. Res.* **103**, 10,859–10,873.

Goodman. J., Toon, O. B., Pueschel, R. F., Snetsinger, K. G. and Verma, S. 1989. Antarctic stratospheric ice crystals. *J. Geophys. Res.* **94**, 16,449–16,457.

Hamill, P., Tabazadeh, Kinne, S., Toon, O. B. and Turco, R. P. 1996. On the growth of ternary system $HNO_3/H_2SO_4/H_2O$ aerosol particles in the stratosphere. *Geophys. Res. Lett.* **23**, 753–756.

Hanson, D. and Mauersberger, K. 1988. Laboratory studies of the nitric acid trihydrate: implications for the south polar stratosphere. *Geophys. Res. Lett.* **15**, 855–858.

Hofmann, D. J. and Deshler, T. 1991. Stratospheric cloud observations during formation of the antarctic ozone hole in 1989. *J. Geophys. Res.* **96**, 2897–2912.

Iraci, L. T., Middlebrook, A. M., Wilson, M. N. and Tolbert, M. A. 1994. Growth of nitric acid hydrates on thin sulfuric acid films. *Geophys. Res. Lett.* **21**, 867–870.

Kent, G. S., Poole, L. R., McCormick, M. P., Schaffner, S. K., Hunt, W. H. and Osborn, M. T. 1990. Optical backscatter characteristics of Arctic polar stratospheric clouds. *Geophys. Res. Lett.* **17**, 377–380.

Klett, D. J. 1981. Stable analytical inversion solution for processing lidar returns. *Appl. Optics* **20**, 211–220.

Klett, J. D. 1985. Lidar inversion with variable backscattering/extinction ratio. *Appl. Optics* **22**, 1638–1645.

Koehler, B. G., Middlebrook, A. M. and Tolbert, M. A. 1992. Characterisation of model polar stratospheric clouds films using Fourier transform infrared spectroscopy and temperature programmed desorption. *J. Geophys. Res.* **97**, 8065–8074.

Koop, T., Biermann, U. M., Raber, W., Luo, B. P., Crutzen, P. J. and Peter, T. 1995. Do stratospheric aerosol droplets freeze above the ice frost point? *Geophys. Res. Lett.* **22**, 917–920.

Koop, T., Carslaw, K. S. and Peter, T. 1997. Thermodynamic stability and phase transition of PSC particles. *Geophys. Res. Lett.* **24**, 2199–2202.

Larsen, N., Knudsen, B. M., Rosen, J. M., Kjome, N. T. and Kyro, E. 1996. Balloonborne backscatter observation of type I PSC formation: inference about physical state from trajectory analysis. *Geophy Res. Lett.* **23**, 1091–1094.

MacKenzie, R., Kulmala, M., Laaksonen, A. and Vesala, T. 1995. On the theories of type I polar stratospheric cloud formation. *J. Geophys. Res.* **100**, 11,275–11,288.

MacKenzie, R., Kulmala, M., Laaksonen, A. and Vesala, T. 1997. Correction to: On the theories of type I polar stratospheric cloud formation. *J. Geophys. Res.* **102**, 19,729–19,730.

MacKenzie, A. R., Laaksonen, A., Batris, E. and Kulmala, M. 1998. The Turnbull correlation and the freezing of stratospheric aerosol droplets. *J. Geophys. Res.* **103**, 10,875–10,884.

Marti, J. and Mauersberger, K. 1993. Laboratory simulation of PSC particle formation. *Geophys. Res. Lett.* **20**, 359–362.

McCormick, M. P., Steele, H. M., Hamill, P., Chu, W. P. and Swissler, T. J. 1982. Polar stratospheric cloud sightings by SAM II. *J. Atmos. Sci.* **39**, 328–331.

McCormick, M. P., Trepte, C. R. and Pitts, M. C. 1989. Persistence of polar stratospheric clouds in the southern polar region. *J. Geophys. Res.* **94**, 11,241–11,251.

Meilinger, S. K., Koop, T., Luo, B. P., Huthwelker, T., Carslaw, K. S., Krieger, U., Crutzen, P. J. and Peter, T. 1995. Size-dependent stratospheric droplet composition in lee wave temperature fluctuations and their potential role in PSC freezing. *Geophys. Res. Lett.* **22**, 3031–3034.

Molina, M. J., Zhang, R., Wooldridge, P. J., McMahon, J. R., Kim, J. E., Chang, H. Y. and Beyer, K. D. 1993. Physical chemistry of the $H_2SO_4/HNO_3/H_2O$ system: implications for polar stratospheric clouds. *Nature* **261**, 1418–1423.

Morandi, M. 1992. *A complete procedure for inverting lidar returns.* Research Report RR/GCF/92.11, available from IROE-CNR, Florence, Italy.

Peter, T., Müller, R. and Crutzen, P. J. 1994. The lifetime of lee-wave-induced ice particles in the Arctic stratosphere: II. Stabilisation due to NAT-coating. *Geophys. Res. Lett.* **21**, 1331–1334.

Poole, L. R., Kent, G. S., McKormick, M. P., Hunt, W. H., Osborne, M. T., Schaffner, S. and Pitts, M. C. 1990. Dual polarization airborne lidar observations, of polar stratospheric cloud evolution. *Geophys. Res. Lett.* **17**, 389–392.

Poole, L. R. and Pitts, M. C. 1994. Polar stratospheric cloud climatology based on stratospheric aerosol measurement II observation from 1978 to 1989. *J. Geophys. Res.* **99**, 13,083–13,089.

Pruppacher, H. R. and Klett, D. J. 1985. *Clouds and precipitation.* D. Reidel, Noerwell, Mass., USA.

Pullen, S. and Jones R. L. 1997. Accuracy of temperatures from UKMO analyses of 1994/95 in the Arctic winter stratosphere. *Geophys. Res. Lett.* **24**, 845–848.

Rosen, J. M., Oltmans, S. J. and Evans, W. F. 1989. Balloon borne observations of PSCs frost point ozone and nitric acid in the North Polar Vortex. *Geophys. Res. Lett.* **16**, 791–794.

Rosen, J. M., Kjome, N. T. and Oltmans, S. J. 1993. Simultaneous ozone and polar stratospheric cloud observations at South Pole station during winter and spring 1991. *J. Geophys. Res.* **98**, 12,741–12,751.

Rosenfield, J. E., Newman, P. A. and Schoeberl, M. R. 1994. Computation of diabatic descent in the stratospheric polar vortex. *J. Geophys. Res.* **99**, 16,677–16,689.

Santacesaria, V., Stefanutti, L., Morandi, M., Guzzi, D. and MacKenzie, A. R. 1999. Two-year (1996/1997) ozone DIAL measurement over Dumont d'Urville (Antarctica). *Geophys. Res. Lett.* **26**, 463–466.

Schoeberl, M. R. and Hartmann, D. L. 1991. The dynamics of the stratospheric polar vortex and its relation to springtime ozone depletions. *Science* **251**, 46–52.

Solomon, S., Garcia, R. R., Rowland, F. S. and Wuebbles, D. J. 1986. On the depletion of Antarctic ozone. *Nature* **321**, 755–758.

Stefanutti, L., Morandi, M., del Guasta, M., Godin, S., Megie, G., Brechet, J. and Piquard, J. 1991. Polar stratospheric cloud observations over the Antarctic continent at Dumont D'Urville. *J. Geophys. Res.* **96**, 12,975–12,987.

Stefanutti, L., Castagnoli, F., Del Guasta, M., Morandi, M., Sacco, V. M., Zuccagnoli, L., Godin, S., Megie, G. and Porteneuve, J. 1992. The Antarctic ozone lidar system. *Appl. Phys. B* **55**, 3–12.

Stefanutti, L., Morandi, M., Del Guasta, M., Godin, S. and David, C. 1995. Unusual PSC observed by LIDAR in Antartica. *Geophys. Res. Lett.* **22**, 2377–2380.

Stefanutti, L., MacKenzie, A. R., Balestri, S., Khattatov, V., Fiocco, G., Kyro, E. and Peter, T. 1999. APE-POLECAT — Rationale, Road Map and Summary of Measurements. *J. Geophys. Res.* **104**, 23,941–23,959.

Stein, B., Del Guasta, M., Kolenda, J., Morandi, M., Rairoux, P., Stefanutti, L. and Wolf, J. P. 1994. Stratospheric aerosol size distribution from multispectral lidar measurements at Sodankylä during EASOE. *Geophys. Res. Lett.* **21**, 1311–1314.

Stein, B., Wedekind, C., Wille, H., Immler, F., Müller, M., Wöste, L., Del Guasta, M., Morandi, M., Stefanutti, L., Antonelli, A., Agostini, P., Rizi, V., Redaelli, G., Mitev, V., Matthey, R., Kivi, R. and Kyrö, E. 1999. Optical classification, existence temperature and co-existence of different PSC types. *J. Geophys. Res.* **104**, 23,983–23,993.

Tabazadeh, A., Turco, R. P., Drdla, K. and Jacobson, M. Z. 1994. A study of type I polar statospheric cloud formation. *Geophys. Res. Lett.* **21**, 1619–1622.

Tabazadeh, A., Toon, O. B., Gary, B. L., Bacmeister, J. T. and Schoeberl, M. R. 1996. Observational constraints on the formation of Type Ia polar stratospheric clouds. *Geophys. Res. Lett.* **23**, 2109–2112.

Toon, O. B., Hamill, P., Turco, R. P. and Pinto, J. 1986. Condensation of HNO_3 and HCl in the winter polar strtosphere. *Geophys. Res. Lett.* **13**, 1284–1287.

Toon, O. B., Browell, E. V., Kinne, S. and Jordan, J. 1990. An analysis of lidar observations of polar stratospheric clouds. *Geophys. Res. Lett.* **17**, 393–396.

Toon, O. B., Turco, R. P. and Hamill, P. 1990b. Denitrification mechanism in the solar stratosphere. *Geophys. Res. Lett.* **17**, 445–448.

Tsias, A., Wirth, M., Carslaw, K. S., Biele, J., Mehrtens, H., Reichardt, J., Wedekind, C., Weiss, V., Renger, W., Neuber, R., VonZahn, U., Stein, B., Santacesaria, V., Stefanutti, L., Fierli, F., Bacmeister, J. and Peter, T. 1999. Aircraft lidar observations of an enhanced type Ia polar stratospheric clouds during APE-POLECAT. *J. Geophys. Res.* **104**, 23,961–23,969.

Tuck, A. F., Baumgardner, D., Chan, K. R., Dye, J. E., Elkins, J. W., Hovde, S. J., Kelly, K. K., Loewenstein, M., Margitan, J. J., May, R. D., Podolske, J. R., Proffitt, M. H., Rosenlof, K. H., Smith, W. L., Webster, C. R. and Wilson, J. C. 1997. The Brewer–Dobson circulation in the light of high altitude in situ aircraft observations. *Quart. J. Roy. Meteorol. Soc.* **123**, 1–69.

Turco, R. P., Toon, O. B. and Hamill, P. 1989. Heterogeneous physicochemistry of the polar ozone hole. *J. Geophys Res.* **94**, 16,493–16,510.

Wofsy, S. C., Salawitch, R. J., Yatteau, J. H., McElroy, M. B., Gandrud, B. W., Dye, J. E. and Baumgardner, D. 1990. Condensation of HNO_3 on falling ice particles: mechanism for denitrification of the polar stratosphere. *Geophys. Res. Lett.* **17**, 449–452.

Worsnop, D. R, Fox, L. E., Zahniser, M. S. and Wofsy, C. S. 1993. Vapour pressure of solid hydrates of nitric acid: implications for polar stratospheric clouds. *Science* **259**, 71–74.